Applied Physics B (2024) 130:156
https://doi.org/10.1007/s00340-024-08297-8

Applied Physics B
Lasers and Optics

RESEARCH

Multiphoton absorption with Laguerre-Gaussian beams

Ferhat Kessi[1]

Received: 2 May 2024 / Accepted: 6 August 2024 / Published online: 9 August 2024

Abstract
Laguerre-Gaussian beams possess a unique transverse mode structure defined by the orbital l and radial m mode numbers, offering promising potential for controlling nonlinear optical interactions. This comprehensive study aims to elucidate the crucial influence of this transverse mode structure on the nonlinear absorption processes. We first established a rigorous theoretical framework by deriving analytical expressions describing the behavior of the Open Z-scan normalized optical transmittance for an arbitrary nth-order nonlinear process under the weak nonlinearity approximation, accounting for the transmitted optical intensity, power, and their dependency on the beam's transverse mode profile. In the numerical simulations, we focused on the specific case of second-order ($n = 2$) nonlinear absorption. Subsequently, detailed numerical simulations were employed to systematically analyze the intricate interplay between the l and m mode indices and their impact on the transmittance characteristics. By precisely varying these indices, we investigated how the observed transmission profiles were affected, revealing distinct behaviors for different Laguerre-Gaussian modes. When only m increases, absorption decreases due to the wider transverse energy spread, while varying l leads to a non-monotonic trend involving intense lobes. Remarkably, simultaneously increasing both l and m systematically enhances absorption through constructive interference of the helical and ring-like structures.

1 Introduction

Nonlinear absorption is a phenomenon where the absorption coefficient of a material depends on the intensity of the incident light. This nonlinear behavior arises from various mechanisms such as multiphoton absorption, saturated absorption, or free-carrier absorption [1, 2]. In our work, we focus on multiphoton absorption, where multiple photons are simultaneously absorbed to excite an atom or molecule to a higher energy level, which is only possible at high light intensities. Saturated absorption occurs when the ground state population is depleted at high intensities, leading to decreased absorption. Free-carrier absorption involves the absorption of photons by free carriers generated through other nonlinear processes. Multiphoton absorption has several notable applications including multiphoton microscopy for high-resolution fluorescence imaging of biological tissues [3], 3D microfabrication through localized two-photon polymerization of photoresists [4] and high-density 3D optical data storage by two-photon writing [5].

Investigating multiphoton absorption processes experimentally requires advanced techniques capable of probing nonlinear optical phenomena at high intensities. A widely employed method is the Z-scan technique, introduced by Sheik-Bahae et al. in 1989 [6]. The open-aperture Z-scan configuration is particularly well-suited for measuring nonlinear absorption coefficients, including multiphoton absorption cross-sections. In an open-aperture Z-scan setup, a focused laser beam is translated along its propagation axis (the z-axis) through a thin sample of the material under study. The transmittance of the sample is recorded as a function of the sample position z relative to the beam focus [7]. As the sample crosses the focal plane, the peak intensity experienced by the sample changes, leading to a variation in the measured transmittance due to the intensity-dependent nonlinear absorption. By fitting the recorded open-aperture Z-scan trace to an appropriate theoretical model, the nonlinear absorption coefficient can be extracted. Crucially, the open-aperture configuration is insensitive to nonlinear refraction effects, ensuring that the measured nonlinearity is solely due to absorption mechanisms. Other techniques employed to characterize

✉ Ferhat Kessi
ferhat.kessi@univ-bejaia.dz

[1] Department of Technology, Campus El Kseur, A. Mira University of Bejaia, 06003 Bejaia, Algeria

multi-photon absorption include nonlinear transmission measurements [8], pump-probe spectroscopy [9], and two-photon excited fluorescence [10]. However, the open-aperture Z-scan method offers several advantages, such as simplicity, sensitivity, and the ability to separate different nonlinear absorption processes based on their intensity dependence [11]. The Z-scan technique has been applied to study multiphoton absorption in a wide range of materials, including semiconductors [12], organic molecules [13], nanostructures [14], and biological samples [15].

In theoretical and experimental studies of multiphoton absorption, the choice of the incident beam is crucial, often guided by research objectives or desired applications [16]. Theoretical models and numerical simulations predict the behavior of these beams in nonlinear media, considering beam parameters, nonlinear material properties, and underlying multiphoton absorption mechanisms [17]. Theoretical models of nonlinear absorption in Z-scan measurements can be categorized into two main groups based on the spatial profile of the incident laser beam [18]. Analytical expressions for the normalized optical transmission have been derived as a function of beam parameters and material properties for both categories. The first category assumes a circular Gaussian beam profile [6, 11, 19–22] to describe nonlinear absorption processes up to a specific order or a generalized nonlinear process of arbitrary order. The second category utilizes an elliptical Gaussian beam profile [23], with only one model proposed for an arbitrary nth-order nonlinear process.

While this theoretical framework accounts for spatially asymmetric laser beams and their associated nonlinear responses, further development is needed for other beam profiles commonly encountered. The formulation of additional models for spatially structured beams beyond circular and elliptical Gaussian cases remains necessary to fully describe nonlinear absorption using the Z-scan technique under diverse excitation conditions. The use of Laguerre-Gaussian (LG) beams as incident beams is particularly significant and potentially advantageous. LG beams possess a ring-shaped transverse intensity profile with an azimuthal phase dependence, resulting in an optical vortex at the beam center [24]. This unique intensity distribution can lead to enhanced nonlinear absorption processes due to the high intensity gradients present in the beam profile. Furthermore, controlling the beam parameters, such as the radial and azimuthal mode indices [25], allows tailoring the intensity distribution and exploring its influence on the nonlinear absorption dynamics. These characteristics of LG beams offer increased sensitivity in Z-scan measurements, provide complementary information to traditional Gaussian beam experiments, and are particularly relevant for studying structured light interactions in nonlinear optics.

In the concluding part of this introduction, we will discuss the focus of our work, which aims to develop theoretical models for arbitrary order nonlinear absorption processes in the weak nonlinearities regime, taking into account linear absorption within the framework of the open-aperture Z-scan experiment. The material under study is considered thin, and Laguerre-Gaussian (LG) beams are employed as incident beams. It is important to note that, to the best of our knowledge, this specific approach has not been previously explored in the literature, as our extensive bibliographic research did not uncover any prior work addressing this particular combination of nonlinear absorption order, linear absorption, open-aperture Z-scan, and LG beam illumination.

The paper is divided into two main sections. Firstly, we develop the theoretical model through multiple steps. We begin by deriving expressions for the transmitted optical intensity, followed by the transmitted optical power. Finally, we obtain an expression for the normalized optical transmittance. This first section outlines the full mathematical framework. In the second section, we perform some numerical simulations to analyze the influence of the radial and azimuthal mode indices on the optical transmittance. Specifically, we computationally study how variations in these mode indices affects the transmittance behavior. These simulations provide insights into how the different Laguerre-Gaussian modes are transmitted according to the model developed in the initial theoretical section.

2 Theoretical model

Laguerre-Gaussian beams (LG) are a family of solutions to the paraxial wave equation in cylindrical coordinates [24]. They have a doughnut-shaped intensity profile and an azimuthal phase dependence. The order of the Laguerre-Gaussian beam modes are specified by the indices l and m. The indice l is called the azimuthal mode order, as it determines the azimuthal phase structure and orbital angular momentum. The indice m is called the radial mode order, as it governs the radial nodes and intensity rings in the profile. Laguerre-Gaussian beams can be produced experimentally by passing a laser beam through a spiral phase plate [26], which imparts the required azimuthal phase profile. They can also be generated using spatial light modulators or cylindrical mode converters [27]. Due to their orbital angular momentum, Laguerre-Gaussian beams have potential applications in optical tweezers and spanners for manipulating microscopic objects [28]. They are also being investigated for use in optical communication networks as a way to increase data transmission capacity [29].

Considering a Laguerre-Gaussian laser beam of order (l, m) propagating along the (OZ) axis and incident on a thin

nonlinear material sample, the complex electric field amplitude associated with this beam can be described as [30]:

$$E_{lm}(x,y,z,t) = E_0(t)\frac{W_0}{W(z)}\left(\frac{\rho}{W(z)}\right)^l L_m^l\left(\frac{2\rho^2}{W^2(z)}\right)\exp\left(-\frac{\rho^2}{W^2(z)}\right)\exp\left(-j\left[kz + l\phi - (1+l+2m)\zeta(z) + \frac{k\rho^2}{2R(z)}\right]\right) \quad (1)$$

where $E_0(t)$ is the time-dependent amplitude at the beam center or focus containing temporal profile $h(t)$ of the pulse,$W_0/W(z)$ is an amplitude scaling factor accounting for beam width $W(t)$ variation with propagation distance,$(\rho/W(z)^l$ describes the radial polarization dependence with ρ as the radial cylindrical coordinate, L_m^l is the associated Laguerre polynomial of order l and m, $\exp\left(-\rho^2/W^2(z)\right)$ gives the Gaussian beam intensity profile. The complex field equation also contains important phase terms. The quantity kz models the longitudinal wave number as the beam travels along z with k the wavenumber in free space, the azimuthal phase $l\phi$ imparts orbital angular momentum and $\zeta(z)$ is the Gouy phase from beam focusing or defocusing. The radial curvature phase $\left(k\rho^2/2R(z)\right)$ accounts for the locally varying radius of curvature $R(z)$ of the wavefront. These phase components fully characterize the three-dimensional helical wavefront of the LG mode.

The parameters $W(z)$, $R(z)$ and $\zeta(z)$ are given by the following relations:

$$W(z) = W_0\left(1 + \left(\frac{z-z_0}{z_R}\right)^2\right)^{\frac{1}{2}} \quad (2a)$$

$$R(z) = z\left(1 + \left(\frac{z-z_0}{z_R}\right)^2\right) \quad (2b)$$

$$\zeta(z) = \arctan\left(\frac{z}{z_R}\right) \quad (2c)$$

where W_0 is the waist radius, which represents the minimum beam width, z_0 is the axial location of the beam waist and z_R is the Rayleigh range. It corresponds to the distance from z_0 over which the initial beam divergence occurs. Specifically, z_R is the distance required for the beam radius $W(z)$ to increase by a factor of $\sqrt{2}$ compared to the waist radius W_0. The Rayleigh range is given by the following formula:

$$z_R = \frac{\pi W_0^2}{\lambda} \quad (2d)$$

where λ is the wavelength of the laser beam. Although the full expression contains a time-dependent term $\exp(-j\omega t)$, Equation (1) omits this factor, with ω representing the angular frequency of the Laguerre-Gaussian beam. The angular frequency ω is connected to the wavelength λ via the usual electromagnetic wave equation $\omega = 2\pi c/\lambda$. In this equation, c symbolizes the velocity of light in a vacuum.

When solely considering a nonlinear absorption process of arbitrary order n, accounting for linear absorption and within the slowly varying envelope approximation, the behavior of an intensity-modulated Gaussian beam propagating inside a thin nonlinear material can be characterized. The beam intensity $I(x,y,z\prime,t)$ varies with the propagation distance z′ inside the sample according to a first-order nonlinear differential equation [2]:

$$\frac{dI(x,y,z\prime,t)}{dz\prime} = -\alpha_0 I(x,y,z\prime,t) - \alpha_n I^n(x,y,z\prime,t) \quad (3)$$

This equation describes how the beam intensity changes over $z\prime$ due to both linear and nonlinear absorption effects. The linear absorption is represented by the term $-\alpha_0 I(x,y,z\prime,t)$, where α_0 is the corresponding coefficient. Nonlinear absorption of order n is contained in the factor $-\alpha_n I^n(x,y,z\prime,t)$, with α_n as the nonlinear absorption coefficient of order n.

Upon inspection, equation (3) can be recognized as a first-order nonlinear ordinary differential equation in the form of Bernoulli's equation. By considering the relevant boundary condition $I(z\prime=0) = I_{inc}$, which denotes the incident intensity at the entrance plane of the material, and Making the substitution $z\prime = L$, where L is the geometrical thickness of the sample, allows solving for the transmitted intensity at the exit plane, It is shown that the transmitted optical intensity is given by the relationship [21–23]:

$$I_{out}^{(n)}(x,y,z,t) = \frac{I_{inc}(x,y,z,t)\exp\left(-\alpha_0 L\right)}{\left[1 + (n-1)\alpha_n L_{eff}^{(n-1)} I_{inc}^{n-1}(x,y,z,t)\right]^{\frac{1}{n-1}}} \quad (4)$$

The transmitted intensity expression $I_{out}^{(n)}(x,y,z,t)$ provides the local field amplitude as a function of input beam parameters and material properties, where z denotes the position of the nonlinear optical material relative to the laboratory reference frame, the solution involves the effective sample thickness of order n, $L_{eff}^{(n-1)}$, and the optical incident intensity,$I_{inc}^{n-1}(x,y,z,t)$. These parameters are described by the following expressions:

$$L_{eff}^{(n-1)} = \frac{1 - \exp\left[-(n-1)\alpha_0 L\right]}{(n-1)\alpha_0} \quad (5)$$

$$I_{inc,lm}(\rho,\phi,z,t) = \left|E_{l,m}(\rho,\phi,z,t)\right|^2 = I_0(t)\left(\frac{W_0}{W(z)}\right)^2\left(\frac{\rho}{W(z)}\right)^{2l}\left[L_m^l\left(\frac{2\rho^2}{W^2(z)}\right)\right]^2\exp\left(-\frac{2\rho^2}{W^2(z)}\right) \tag{6}$$

Now, we apply the weak nonlinearity approximation to simplify the expression for transmitted optical intensity. Specifically, we are considering a material that exhibits an nth-order nonlinear absorption process. Typically, the intensity required to drive such a process efficiently increases with the order of the nonlinearity. For an excitation intensity sufficient to induce only the nth-order effect, the probability of simultaneously generating nonlinearities of even higher orders $(n+1)$ and above remains relatively small. This is due to the sharp rise in intensity needed for higher-order processes. While minor higher-order interactions may still occur, their overall contribution becomes negligible compared to the dominant nth-order term. Through applying the weak nonlinearity constraint, we can neglect higher-order terms above $n+1$ in our theoretical analysis. Prior studies have established that this approximation can be expressed quantitatively through a relationship between optical intensity and order of the nonlinearity [23]. Specifically, the required intensity was shown to scale as:

$$\frac{\alpha_n}{\alpha_0} I_{inc,lm}^{n-1} \ll 1 \tag{7}$$

Using this approximation, all terms of order higher than 2 can now be neglected in the Taylor series expansion of the denominator of equation (4). This leads directly to a simplified expression for the transmitted optical intensity. Expanding only to second order yields:

$$I_{out,lm}^{(n)}(\rho,\phi,z,t) = I_{inc,lm}(\rho,\phi,z,t)\exp\left(-\alpha_0 L\right)\left[1-\alpha_n L_{eff}^{(n-1)} I_{inc,lm}^{n-1}(\rho,\phi,z,t)\right] \tag{8}$$

Having derived the simplified expression for transmitted optical intensity using the weak nonlinearity approximation, we can now relate this to the transmitted optical power output. To calculate the power, we must integrate the transmitted intensity over the entire beam cross-section at the exit plane. By integrating this intensity distribution, we obtain the overall power output according to:

$$P_{out,lm}^{(n)}(z,t) = \int_{-\infty}^{+\infty}\int_{-\infty}^{+\infty} I_{out}(\rho,\phi,z,t)dxdy = e^{-\alpha_0 L}\left\{\int_{-\infty}^{+\infty}\int_{-\infty}^{+\infty} I_{inc,lm}(x,y,z,t)dxdy - \alpha_n L_{eff}^{(n-1)}\int_{-\infty}^{+\infty}\int_{-\infty}^{+\infty} I_{inc,lm}^{n}(x,y,z,t)dxdy\right\} \tag{9}$$

To calculate the transmitted optical power, we divided its expression into two contributions. Expressing this in polar coordinates, the first contribution is given by:

$$\begin{aligned}&\int_{-\infty}^{+\infty}\int_{-\infty}^{+\infty} I_{inc,lm}(x,y,z,t)dxdy \\ &= I_0(t)\left(\frac{W_0}{W(z)}\right)^2\int_0^{2\pi}\int_0^{+\infty}\left(\frac{\rho}{W(z)}\right)^{2l}\left[L_m^l\left(\frac{2\rho^2}{W^2(z)}\right)\right]^2\exp\left(-\frac{2\rho^2}{W^2(z)}\right)\rho d\rho d\phi \\ &= 2\pi I_0(t)\left(\frac{W_0}{W(z)}\right)^2\int_0^{+\infty}\left(\frac{\rho^2}{W^2(z)}\right)^{l}\left[L_m^l\left(\frac{2\rho^2}{W^2(z)}\right)\right]^2\exp\left(-\frac{2\rho^2}{W^2(z)}\right)\rho d\rho\end{aligned} \tag{10}$$

To evaluate the integral appearing in relation (10), we performed the following change of variables:

$$u = \frac{2\rho^2}{W^2(z)} \rightarrow du = 4\frac{\rho d\rho}{W^2(z)} \rightarrow \rho d\rho = \frac{W^2(z)du}{4} \tag{11}$$

where we introduced the dimensionless variable u. The expression (10) then becomes:

$$\int_{-\infty}^{+\infty}\int_{-\infty}^{+\infty} I_{inc,lm}(x,y,z,t)dxdy = 2\pi I_0(t)\left(\frac{W_0}{W(z)}\right)^2\frac{W^2(z)}{4}\int_0^{+\infty}\left(\frac{u}{2}\right)^l\left[L_m^l(u)\right]^2\exp(-u)du \tag{12}$$

By utilizing the properties of generalized Laguerre polynomials [31], one was able to obtain the following result:

$$\int_{-\infty-\infty}^{+\infty+\infty} I_{inc,lm}(x,y,z,t)dxdy$$
$$= \frac{\pi}{2} I_0(t) W_0^2 \left(\frac{1}{2}\right)^l \int_0^{+\infty} u^l \left[L_m^l(u)\right]^2 \exp(-u)du$$
$$= \frac{\pi}{2^{l+1}} I_0(t) W_0^2 \frac{\Gamma(l+m+1)}{m!} \tag{13}$$

To evaluate the second integral appearing in relation (9), we followed the same procedure. Expressing this in polar coordinates, the integral is presented as:

$$\int_{-\infty-\infty}^{+\infty+\infty} I_{inc,lm}^n(x,y,z,t)dxdy$$
$$= I_0^n(t)\left(\frac{W_0}{W(z)}\right)^{2n} \int_0^{2\pi}\int_0^{+\infty} \left(\frac{\rho}{W(z)}\right)^{2nl}$$
$$\left[L_m^l\left(\frac{2\rho^2}{W^2(z)}\right)\right]^{2n} \exp\left(-\frac{2n\rho^2}{W^2(z)}\right)\rho d\rho d\phi$$
$$= 2\pi I_0^n(t)\left(\frac{W_0}{W(z)}\right)^{2n} \int_0^{+\infty} \left(\frac{\rho^2}{W^2(z)}\right)^{nl}$$
$$\left[\left(L_m^l\left(\frac{2\rho^2}{W^2(z)}\right)\right)^n\right]^2 \exp\left(-\frac{2n\rho^2}{W^2(z)}\right)\rho d\rho \tag{14}$$

By using the change of variables (11), this integral takes the following form:

$$\int_{-\infty-\infty}^{+\infty+\infty} I_{inc,lm}^n(x,y,z,t)dxdy = \frac{\pi}{2^{nl+1}} I_0^n(t)\left(\frac{W_0^{2n}}{W^{2n-2}(z)}\right)\int_0^{+\infty} (u)^{nl}\left[\left(L_m^l(u)\right)^n\right]^2 \exp(-nu)du = \frac{\pi}{2^{nl+1}} D(n,l,m) I_0^n(t)\left(\frac{W_0^{2n}}{W^{2n-2}(z)}\right) \tag{15}$$

where we have introduced the quantity $D(n,l,m)$ defined by:

$$D(n,l,m) = \int_0^{+\infty} (u)^{nl}\left[\left(L_m^l(u)\right)^n\right]^2 \exp(-nu)du \tag{16}$$

This quantity $D(n,l,m)$ is dimensionless and only depends on the indices n, l and m. It does not depend on the parameters of the Gaussian beam or the properties of the material and can be evaluated numerically for different values of the indices.

Substituting relations (13) and (15) into the relation (9) then provides the expression for the transmitted optical power as:

$$P_{out,lm}^{(n)}(z,t) == \exp(-\alpha_0 L)\left\{\frac{\pi}{2^{l+1}} I_0(t) W_0^2 \frac{\Gamma(l+m+1)}{m!}\right.$$
$$\left. -\alpha_n L_{eff}^{(n-1)} \frac{\pi}{2^{nl+1}} D(n,l,m) I_0^n(t)\left(\frac{W_0^{2n}}{W^{2n-2}(z)}\right)\right\}$$
$$= P_{inc,lm}(t)\exp(-\alpha_0 L)\left\{1 - \alpha_n L_{eff}^{(n-1)} I_0^{n-1}(t)\right.$$
$$\left.\frac{2^{l-nl} m! D(n,l,m)}{\Gamma(l+m+1)}\left(\frac{W_0}{W(z)}\right)^{2n-2}\right\} \tag{17}$$

where we have introduced the quantity $P_{inc,lm}(t)$ representing the incident optical power, given by the following expression:

$$P_{inc,lm}(t) = \frac{\pi}{2^{l+1}} I_0(t) W_0^2 \frac{\Gamma(l+m+1)}{m!} \tag{18}$$

To complete the model development, we evaluate the normalized optical transmittance. This quantity represents the fraction of incident optical power that is transmitted through the material. It is defined as the ratio of the transmitted optical power to the maximum incident power. The normalized optical transmittance can be written as:

$$T_{lm}^{(n)}(z) = \frac{\int_{-\infty}^{+\infty} P_{out}^{(n)}(z,t)dt}{\int_{-\infty}^{+\infty} P_{inc}(t)dt} \tag{19}$$

Through applying the expressions derived for the incident and transmitted optical powers, as given in relations (17) and (18), and explicitly defining the axial dependence of the beam width as expressed in relation (2a), we obtain the following for the normalized optical transmittance:

$$T_{lm}^{(n)}(z) = \exp(-\alpha_0 L)\left[1 - \frac{\frac{2^{l-nl} m! D(n,l,m)}{\Gamma(l+m+1)} \alpha_n L_{eff}^{(n-1)} I_0^{n-1}}{\left(1+\left(\frac{z}{z_R}\right)^2\right)^{n-1}} \frac{\int_{-\infty}^{+\infty} h^n(t)dt}{\int_{-\infty}^{+\infty} h(t)dt}\right] \tag{20}$$

where I_0 epresents the on-axis intensity of the incident beam at the focus, specifically $I_0 = I(0,0)$. The relation (20) can also be rewritten in the following form:

$$T_{lm}^{(n)}(z) = \exp(-\alpha_0 L)\left[1 - \frac{\alpha_n F_{l,m}^{(n)}}{\left(1+\left(\frac{z-z_0}{z_R}\right)^2\right)^{n-1}}\right] \tag{21}$$

where we have introduced the parameter $F_{l,m}^{(n)}$, which is defined as:

$$F_{l,m}^{(n)} = \frac{m!D(n,l,m)L_{eff}^{(n-1)}I_0^{n-1}\int_{-\infty}^{+\infty} h^n(t)dt}{2^{l(n-1)}\Gamma(l+m+1)\int_{-\infty}^{+\infty} h(t)dt} \tag{22}$$

For the special but practical case where the pulse has a Gaussian temporal profile, we have:

$$h(t) = \exp\left(-t^2\right) \tag{23a}$$

$$\int_{-\infty}^{+\infty} h(t)dt = \pi \tag{23b}$$

$$\int_{-\infty}^{+\infty} (h(t))^n dt = \frac{\pi}{\sqrt{n}} \tag{23c}$$

$$F_{lm}^{(n)} = \frac{m!D(n,l,m)L_{eff}^{(n-1)}I_0^{n-1}}{2^{l(n-1)}\Gamma(l+m+1)\sqrt{n}} \tag{23d}$$

In the even more specialized scenario where the incident laser beam has both a Gaussian spatial profile (fundamental mode $l = m = 0$) and a Gaussian temporal pulse profile, the expression for $F_{lm}^{(n)}$ simplifies to:

$$F_{00}^{(n)} = \frac{D(n,0,0)L_{eff}^{(n-1)}I_0^{n-1}}{\sqrt{n}} = \frac{L_{eff}^{(n-1)}I_0^{n-1}}{n\sqrt{n}} \tag{24a}$$

where :

$$D(n,0,0) = \int_0^{+\infty} \exp(-nu)du = \frac{1}{n} \tag{24b}$$

We arrive at the same result that we had previously established in our earlier works [23]. By reproducing this prior result for a Gaussian beam, it verifies the validity of our current model. Retrieving the expression we had previously derived confirms the consistency and correctness of our treatment, especially when a more general Hermite-Gaussian beam reduces down to the simpler Gaussian case.

The transmittance expression we have derived provides a theoretical foundation that can be leveraged for analyzing experimental laser beam propagation measurements. Notably, it enables fitting the expression to results from Z-scan experiments, which probe materials by measuring transmittance changes from nonlinear absorption. By comparing the recorded Z-scan transmission curves against our theoretical transmittance formula, both the absorption coefficient and the actual incident beam profiles can be extracted. This allows determining crucial optical properties of the samples under study.

Table 1: Parameters $D(2,l,m)$ and $F_{lm}^{(2)}$ for different (l,m) mode indices of the incident Laguerre-Gaussian beam

m	l	$D(2,l,m)$	$F_{lm}^{(2)}(GW/cm)$
0	0	0.5	7.072
1	0	0.25	3.536
2	0	0.171	2.418
3	0	0.132	1.867
0	1	0.25	1.768
0	2	0.75	1.325
0	3	5.625	1.657
1	1	0.625	2.210
2	2	13.99	4.121
3	3	1031.83	15.202

3 Simulations

In the final part of our paper, we will perform simulations utilizing the derived transmittance relation (21) to study the influence of the beam modal indices l and m on nonlinear absorption processes. We will focus on scenario that have been extensively studied experimentally, namely second-order nonlinear absorption ($n = 2$).

To study the influence of the (l,m) indices of Laguerre-Gaussian (LG) beams on nonlinear absorption, we consider the following combinations:

- The fundamental Gaussian mode for a reference (0,0).
- Modes with $l = 0$ and varying m to study the effect of radial nodes.
- Modes with $m = 0$ and varying l to study the effect of the ring structure.
- Modes with $l = m$ to study cases where there are both radial nodes and a ring structure.

The simulations were performed using the parameter values [20]. We assume the pulse has a Gaussian temporal profile, set the beam waist position $z_0 = 0$, and neglect linear absorption ($\alpha_0 = 0$). In Table 1, we have listed the values of the parameters $D(2,l,m)$ and $F_{lm}^{(2)}$ for different values of the indices (l,m) of the incident Laguerre-Gaussian beam. These values correspond to the cases mentioned below.

Figure 1 graphically depicts the Z-scan signatures or traces for the second-order ($n = 2$) absorption process for different values of the beam indices (l,m). Figure 1a shows the variation of the transmittance for $l = 0$, where the radial mode number m is varied from 0 to 3. In Figure 1b, the radial mode is fixed at $m = 0$, and the orbital angular momentum number l is varied from 0 to 3. On the other hand, Figure 1c

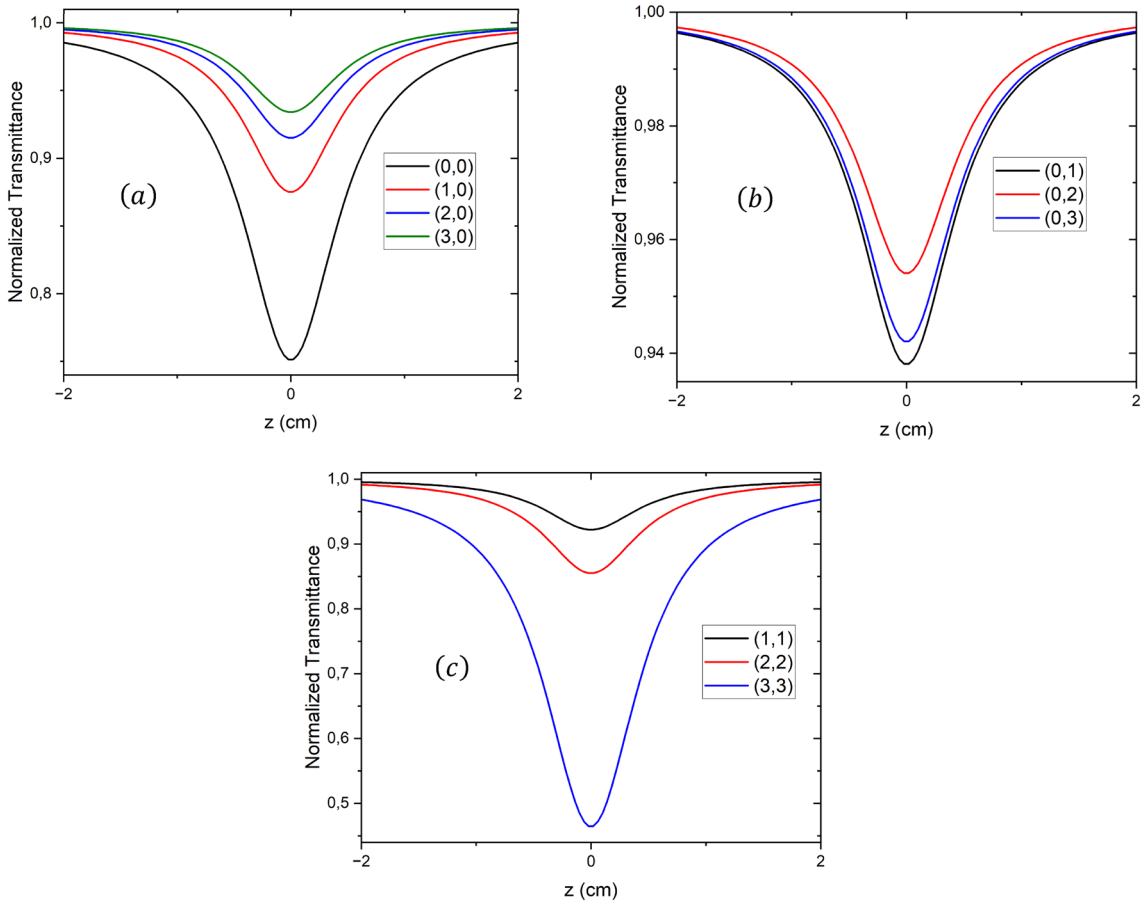

Figure 1: Z-scan signatures for second-order ($n = 2$) absorption process of Laguerre-Gaussian beams: **a** Fixed $l = 0$, varying $m = 0$ to 3 **b** Fixed $m = 0$, varying $l = 0$ to 3 **c** Simultaneous variation of l and m for 1 to 3

simultaneously varies both the l and m indices with the same step size from 0 to 3.

Across all the cases presented, we observe the familiar valley shape that is characteristic of nonlinear absorption processes. The normalized optical transmittance decreases, indicating an increase in absorption, as the sample approaches the beam waist located at $z = 0$, where the absorption reaches its maximum. Notably, these curves exhibit symmetry about the $z = 0$ point. This symmetry arises because the intensity distribution of the Laguerre-Gaussian beams is itself symmetric about the beam waist, leading to an equal absorption behavior when the sample is translated equidistantly before or after the focus. As the sample moves away from the beam waist in either direction, the intensity drops, resulting in decreased nonlinear absorption and a recovery in transmittance. The overall shape reflects the nonlinear dependence of the multiphoton absorption process on the peak intensity at the beam focus.

The trends observed in Figure 1a, where the orbital angular momentum number l is fixed at 0 while the radial mode number m is varied from 0 to 3, reveal an intriguing phenomenon. As m increases, the nonlinear absorption, indicated by the depth of the transmittance valley, progressively diminishes. This behavior can be attributed to the transverse intensity distribution of the Laguerre-Gaussian beams. Higher radial mode numbers correspond to beam profiles with an increasing number of concentric rings in the intensity pattern. Consequently, for larger m values, the energy is distributed over a larger area in the transverse plane, leading to a lower peak intensity at the beam center. Since multiphoton absorption scales nonlinearly with intensity, this reduction in peak intensity results in a weaker nonlinear absorption effect. Additionally, the presence of intensity nulls in the higher-order radial modes may also contribute to the decreased absorption by reducing the effective interaction volume. These observations highlight the intricate interplay between the beam's transverse mode structure and the nonlinear optical process, emphasizing the importance of understanding and tailoring the input beam characteristics for optimizing nonlinear optical interactions.

The trends observed in Figure 1b, where the radial mode number m is fixed at 0 while the orbital angular momentum number l is varied, reveal a non-monotonic behavior in the nonlinear absorption. As l increases from 1 to 2, we witness an enhancement in the absorption, indicated by a deeper transmittance valley. However, upon further increasing l to 3, the absorption unexpectedly decreases. This phenomenon can be understood by considering the intricate interplay between the helical wavefront and the resulting transverse intensity distribution associated with different l values. For $l = 1$, the presence of a central vortex due to the phase singularity leads to a reduction in peak intensity, consequently lowering the absorption. As l increases to 2, the intensity redistributes into intense petals or lobes surrounding the central vortex, effectively concentrating the energy into higher intensity regions and enhancing the nonlinear absorption process. However, when l is further increased to 3, the transverse intensity pattern becomes more complex, with additional petals or lobes emerging. While this intricate structure may locally increase the intensity in certain regions, it also leads to a more widespread distribution of the energy over a larger area in the transverse plane. Consequently, the overall peak intensity experienced by the sample decreases, resulting in a reduction in the observed nonlinear absorption for $l = 3$ compared to $l = 2$. This non-monotonic behavior highlights the delicate balance between the beam's orbital angular momentum, the resulting transverse mode structure, and the peak intensity distribution's influence on nonlinear optical processes. It underscores the importance of carefully considering and tailoring the input beam characteristics to optimize or achieve specific nonlinear optical responses, as the interplay between these factors can lead to intricate and sometimes counterintuitive phenomena.

Figure 1c presents a distinct trend when the orbital angular momentum number l and the radial mode number m are varied simultaneously with the same step size. In contrast to the previous cases where either l or m was held constant, we observe a consistent increase in the nonlinear absorption as both indices are incremented together. This behavior can be attributed to the combined effects of the helical wavefront associated with non-zero l values and the radial intensity distribution governed by m. As l increases, the transverse intensity pattern develops more pronounced intense petals or lobes, as previously discussed. Simultaneously increasing m introduces additional concentric rings in the radial intensity profile. The simultaneous variation of l and m leads to a constructive interplay between these two aspects of the transverse mode structure. The intense petals or lobes arising from non-zero l values are further segmented by the concentric rings associated with higher m values. This combined effect effectively concentrates the energy into smaller, higher-intensity regions within the transverse plane. Consequently, as l and m are incremented together, the peak intensity experienced by the sample continues to increase, facilitating stronger multiphoton absorption processes. This results in the observed deepening of the transmittance valley, indicating an enhancement in the overall nonlinear absorption. These observations underscore the intricate relationship between the orbital angular momentum, radial mode structure, and the resulting transverse intensity distribution of Laguerre-Gaussian beams. By tailoring both l and m simultaneously, it becomes possible to sculpt the intensity pattern in a way that optimizes the peak intensity and, consequently, the nonlinear optical response of the system under investigation.

In addition to the observed effects on nonlinear absorption, it is important to note that our Z-scan transmittance curves reveal another interesting phenomenon related to Laguerre-Gaussian beams. As seen in Figure 1a, b, c, the width of the transmittance valleys varies with different combinations of radial (m) and azimuthal (l) mode numbers. This variation in the width of the transmittance dip is directly related to the spatial extent of the nonlinear interaction region and the effective Rayleigh length of the beam. For instance, when both m and l increase simultaneously (Figure 1c), we observe a narrowing of the transmittance valley, indicating a more localized and intense nonlinear interaction. This effect is a consequence of the unique spatial intensity distribution of LG beams, where the combination of helical phase structure and radial intensity variations creates regions of highly concentrated energy. The narrowing of the transmittance valley could have potential advantages in applications requiring precise spatial control of nonlinear interactions, such as high-resolution nonlinear microscopy or selective material processing. Future studies could explore how to optimize this effect by fine-tuning the LG beam parameters for specific applications.

While our simulations demonstrate the potential of LG beams for tailoring nonlinear absorption, it's important to acknowledge the experimental challenges in generating and manipulating these beams. Precise control of both radial and azimuthal mode numbers requires sophisticated optical setups. Factors such as beam distortions, alignment sensitivities, and maintaining beam quality over propagation distances can impact the realization of theoretical predictions in practical settings. Future work should address these challenges to bridge the gap between simulations and experimental implementations.

The properties of LG modes, including mode numbers and polarization, can be tailored for specific MPA applications. Spatial light modulators or q-plates can be employed to generate and dynamically control LG beam parameters. Polarization control, achieved through waveplates or polarization-sensitive elements, adds another dimension for optimizing nonlinear interactions. By combining these techniques, researchers can fine-tune the spatial and

polarization properties of LG beams to maximize desired nonlinear effects or achieve selective excitation in complex media.

The unique characteristics of LG beams in MPA processes open up exciting possibilities for various applications. In laser-based micromachining, the ability to control energy distribution through LG mode selection could enable more precise material removal or modification. For material characterization, the sensitivity of LG beams to nonlinear absorption could enhance the detection of subtle material properties or defects. In multiphoton microscopy, tailored LG beams could improve imaging resolution and contrast by optimizing the excitation volume. These examples highlight the potential of LG beams to advance numerous fields relying on nonlinear optical interactions.

4 Conclusion

In this work, we have undertaken a comprehensive investigation to elucidate the profound influence of the transverse mode structure on nonlinear optical absorption processes involving Laguerre-Gaussian beams. We began by establishing a rigorous theoretical framework under the weak nonlinearity approximation, deriving analytical expressions that collectively describe the behavior of the Open Z-scan normalized optical transmittance for an arbitrary nth-order nonlinear process. This entailed meticulous mathematical formulations accounting for the transmitted optical intensity, power, and their dependency on the beam's transverse mode profile. Building upon this theoretical model, we then employed numerical simulations to systematically analyze the intricate interplay between the radial and azimuthal mode indices and their impact on the transmittance characteristics for the specific case of second-order ($n = 2$) nonlinear absorption. We investigated how precisely varying these mode indices affected the observed transmission profiles. When only the radial number m is increased, a progressive decrease in absorption is observed, due to the more widespread distribution of energy over a larger transverse area, effectively reducing the peak intensity. In contrast, varying the orbital number l leads to a non-monotonic trend, with an initial enhancement in absorption arising from the formation of intense lobes, followed by a decrease at higher l values due to a more complex intensity distribution. Remarkably, when both l and m are increased simultaneously, a systematic improvement in nonlinear absorption is observed. This synergy arises from the constructive interference between the helical wavefront associated with non-zero l and the concentric ring structure governed by m, effectively concentrating the energy into regions of very high intensity. Furthermore, our analysis of the Z-scan transmittance curves revealed a notable variation in the width of the transmittance valleys for different combinations of radial and azimuthal mode numbers. This effect, particularly pronounced when both m and l increase simultaneously, indicates a more localized and intense nonlinear interaction region. The results obtained in this study highlight the crucial influence of the transverse mode structure of the incident Laguerre-Gaussian beams on the behavior and efficiency of multiphoton absorption processes. These findings underscore the critical importance of tailoring the input beam and precisely controlling its transverse mode structure to optimize nonlinear optical interactions. By judiciously manipulating the l and m numbers, it becomes possible to sculpt the intensity distribution in a way that maximizes or minimizes multiphoton absorption, opening new avenues for controlling and optimizing nonlinear optical processes.

Author contribution F. Kessi is the sole author of this manuscript. S.B. conceived the study, developed the theoretical framework, performed the numerical simulations, analyzed the results, and wrote the manuscript.

Data availability No datasets were generated or analysed during the current study.

Declarations

Conflict of interest The authors declare no competing interests.

References

1. R.W. Boyd, *Nonlinear Optics* (Academic Press, New York, 2008)
2. R.L. Sutherland, *Handbook of Nonlinear Optics* (CRC Press, Boca Raton, 2003)
3. K. Mizuta, M. Sato : Neurophotonics **11**, 033406 (2024)
4. L. Florea, E. Blasco, V. Mattoli, Adv. Funct. Mater. **33**, 2305697 (2023)
5. M. Jiang, M. Zhang, X. Li et al., Opto-Electron Eng. **46**, 180649 (2019)
6. M. Sheik-Bahae, A.A. Said, E.W. Van Stryland, Opt. Lett. **14**, 955 (1989)
7. R. Das, M.K. Shukla, Pramana **83**, 985 (2014)
8. M.E. Doroshenko, K.A. Pierpoint, A. Říha, H. Jelínková, Phys. Wave Phenom. **31**, 412 (2023)
9. A. Nabilkova, M. Zhukova, M. Melnik et al., Appl. Phys. B **128**, 8 (2022)
10. A.G. Pelosi, E. Silveira-Alves, L.H. Cocca et al., Molecules **28**, 1572 (2023)
11. M. Sheik-Bahae, A.A. Said, T.H. Wei, D.J. Hagan, E.W. Van Stryland, IEEE J. Quantum Electron. **26**, 760 (1990)
12. N.S. Dutta, J.M.P. Almeida, C.R. Mendonça, C.B. Arnold, Opt. Lett. **45**, 3228 (2020)
13. M. Elkhouly, A.M. Kobaisy, H.B. Ahmed et al., Opt. Quantum Electron. **55**, 11 (2023)
14. K.M. Rahulan, N.A.L. Flower, R.A. Sujatha et al., J. Mater. Sci. Mater. Electron. **29**, 1504 (2017)
15. S. Hussain, W. Du, M. Zhang et al., J. Mater. Chem. B **6**, 1943 (2018)

16. S.S. Patil, K.Y. Khandale, P.T. Takale, M.B. Mane, P.P. Nikam, P.P. Shinde, P.P. Patil, M.V. Takale, S.D. Patil, J. Opt. **52**, 1478 (2023)
17. N. Gupta, J. Opt. **50**, 466 (2021)
18. N. Gupta, Opt. Quantum Electron. **53**, 3274 (2021)
19. M. Sheik-Bahae, A.A. Said, T.H. Wei, D.J. Hagan, E.W. Van Stryland, Proc. SPIE **1438**, 126 (1989)
20. D.S. Côrrea, L. De Boni, L. Misoguti et al., Opt. Commun. **277**, 440 (2007)
21. G. Xing, W. Ji, Y. Zheng, J.Y. Ying, Appl. Phys. Lett. **93**, 241114 (2008)
22. B. Gu, X. Huang, S. Tan et al., Appl. Phys. B **95**, 375 (2009)
23. F. Kessi, N. Hamadouche, J. Nonlinear Opt. Phys. Mater. **28**, 1950004 (2019)
24. D.L. Andrews, *Structured Light and Its Applications: An Introduction to Phase-Structured Beams and Nanoscale Optical Forces* (Academic Press, Burlington MA, 2008)
25. A.V. Volyar, E. Abramochkin, Y. Akimova, M. Bretsko, Opt. Lett. **47**, 2402 (2022)
26. M. Ding, Y. Chen, Y. Zhao et al., Laser Phys. Lett. **16**, 035106 (2019)
27. R. Li, R. Yuan, T. Liu et al., Chin. Opt. Lett. **20**, 120501 (2022)
28. J. Béguin, J. Laurat, X. Luan et al., Proc. Natl. Acad. Sci. U.S.A. **117**, 26109 (2020)
29. D. Briantcev, M.A. Cox, A. Trichili et al., Opt. Express **31**, 28859 (2023)
30. B.E.A. Saleh, M.C. Teich, *Fundamentals of Photonics* (Wiley, New Jersey, 2007)
31. A.D. Polyanin, A.V. Manzhirov, *Handbook of Mathematics for Engineers and Scientists* (Chapman and Hall/CRC, Boca Raton, 2006)